

Benchmark: Tao's symplectic integration method

Matheus J. Lazarotto^{1,2*}, Iberê L. Caldas¹ and Yves Elskens²

1. Instituto de Física, Universidade de São Paulo, Rua do Matão 1371, São Paulo 05508-090, Brazil

2. Aix-Marseille Université, CNRS, UMR 7345 PIIM, F-13397, Marseille cedex 13, France

August 14, 2024

Abstract: A benchmark test was conducted for a new symplectic integration method originally developed by Molei Tao. The method raises interest due to its explicit evolution equation, with applicability to both separable and non-separable Hamiltonian systems, and an easy-to-implement, easily generalizable algorithm. In order to compare the method with other, more well-known methods, namely Störmer-Verlet and Runge-Kutta, we conducted a series of benchmark tests comparing their performance in terms of CPU time, system invariants functions conservation, and numerical symplectic area conservation. Overall, it was found that despite being considerably slower than the more optimized Runge-Kutta-Cash-Karp, Tao's method presents a similar performance to Störmer-Verlet, with the extra perk of being more generic and not requiring the use of implicit equations for the evolution of the equations of motion.

1 Introduction

Whenever one desires to numerically solve a system of differential equations with any integration method, the issue of precision in the solutions achieved is immediately raised. In classical mechanics, the solution of the Hamilton equations of motion is required in order to find the trajectories (orbits) over time from physical models of the most diverse sort. However, the Hamiltonian phase space presents a topological structure such that some quantities are conserved, in particular the symplectic 2-form and other adiabatic invariants [1]. The symplectic 2-form is conserved regardless of the orbit being regular or chaotic, although numerically the latter is not achievable given its sensitive dependency on errors.

Perhaps the most widely known and disseminated methods for solving such equations are those of the Runge-Kutta (RK) family, including variations with fixed and adaptive time-step, such as Cash-Karp [2], Fehlberg [3], and Dormand-Prince [4]. Although useful and remarkably fast, these methods lack the conservation of symplectic area, especially for long-time integrations. Thus, it is commonly required of an integration method to produce solutions that respect this conservation within numerical limits.

For this purpose, the so-called symplectic methods were introduced, which keep a symplectic 2-form conserved with no divergent error by applying a canonical mapping between each discrete time step performed. The simplest of these methods, nonetheless still efficient, may be the Störmer-Verlet one [5]. Despite many others being proposed,

*Contact: matheus_jean_l@hotmail.com

in general, they present harder implementation than those of the RK family, mostly due to their implicit mapping algorithm, thus requiring inversion or root-finding methods to solve at each step and therefore being slower in time performance.

The aim of this report is to divulge and test a new and practical symplectic integration method for both separable and non-separable Hamiltonian systems. The method was originally developed by Molei Tao and a thoroughly detailed description is given in its original reference [6]. Here, the method will be briefly exposed, based on its original presentation, and its performance tested for a separable Hamiltonian systems, a 2D optical lattice model, and non-separable one, the restricted three-body planetary system.

The interest in testing Tao's method is due to its explicit character and easy algorithm implementation, as opposed to the more commonly found symplectic algorithms that are implicit or exclusively explicit only for separable systems (see [6] for references on previous explicit methods). As will be discussed further ahead, although the method does not aim for the fastest performance, at least when compared to traditional RK methods, it presented reasonable conservation of both energy and symplectic area for the 2D lattice system, and good symplectic conservation, but high energy deviations for the three-body model, making it an alternative option for those looking for an easy-to-use method when such features are required.

In the original exposition [6], the method's performance was compared to a 4th order RK and a previous pioneering explicit symplectic method developed by Pihajoki [7], adding a correction for a binding problem, improving reliability for long integration times. Two numerical examples were chosen: the Schwarzschild geodesic problem and a non-integrable system, the turbulent nonlinear Schrödinger equation, presenting better conservation of energy in both cases.

Here further tests will be conducted on two other systems, the classical 2D optical lattice model and the restricted three-body problem. Similar to what was done in the original, a non-symplectic adaptive time-step Runge-Kutta-Cash-Karp (RKCK) and the symplectic Störmer-Verlet methods will be used for comparison. The main tests presented here include different time steps, integration order of Tao's algorithm, binding parameters, and their effect on the conservation of invariant quantities of these systems.

Both systems were chosen for specific reasons, and brief introductions to each one are given in section 3 for the 2D lattice and section 4 for the restricted three-body problem. For the lattice model, long integration times are commonly required in diffusion analysis considering orbits from a mixed phase space, thus presenting chaotic and regular solutions which need to be ascertained for their long-term conservation of constants of motion to ensure statistical precision. Similarly in the restricted three-body problem, long time integration is required to evaluate whether planets or satellites remain in orbit or leave indefinitely. Additionally, for the latter, it is a non-separable dynamical system, thus being able to test Tao's algorithm for one of its main application purpose.

In order to make this text self-contained, section 2 presents a summarized version of the algorithm completely based on the main reference [6], along with the tools used to evaluate the integration performance, regarding the conservation of invariants. Following the final remarks, an appendix shows the code implementation in C/C++ for generic (even) orders. A minimal example of how to use it is provided, along with the exact equations of motion used to allow easy reproduction of the tests made here (parameters and initial conditions are listed throughout the text).

The computational setup used was a Dell Vostro 3470 machine, with an Intel Core i7-8700 CPU (3.20 GHz) and Linux OS (Ubuntu 18.04), running simulations single-threaded

and compiled with GCC++11. To enable complete reproduction of all the results, the original code used is made available at github.com/matheuslazarotto/SymplecticTao.

2 Method

2.1 Tao's symplectic integration method

To integrate a d -degree of freedom Hamiltonian system $H(\vec{q}, \vec{p})$, with \vec{q} and \vec{p} as the d -dimensional position and momentum vectors respectively, Tao's method considers a new expanded Hamiltonian \bar{H} including a new pair of copied variables (\vec{q}_c, \vec{p}_c) , starting from the same initial point ($\vec{q}_c(0) = \vec{q}(0)$, $\vec{p}_c(0) = \vec{p}(0)$) and evolving along with the main variables \vec{q} and \vec{p} from the equations of motion of the extended system:

$$\bar{H}(\vec{q}, \vec{q}_c, \vec{p}, \vec{p}_c) = H_A + H_B + \omega H_C, \quad (1)$$

where $H_A := H(\vec{q}, \vec{p}_c)$ and $H_B := H(\vec{q}_c, \vec{p})$ are copies of the original Hamiltonian function written with interchanged variables; ω is a binding factor and H_C is the coupling perturbation given by:

$$H_C(\vec{q}, \vec{q}_c, \vec{p}, \vec{p}_c) := \frac{\|\vec{q} - \vec{q}_c\|^2}{2} + \frac{\|\vec{p} - \vec{p}_c\|^2}{2}. \quad (2)$$

An integration step of δt in Tao's method is thus made by a map $\phi_2^{\delta t}$ from Hamiltonian 1, written as:

$$\phi_2^{\delta t} := \phi_{H_A}^{\delta t/2} \circ \phi_{H_B}^{\delta t/2} \circ \phi_{\omega H_C}^{\delta t} \circ \phi_{H_B}^{\delta t/2} \circ \phi_{H_A}^{\delta t/2}, \quad (3)$$

where each partial mapping is given by:

$$\phi_{H_A}^{\delta t} := \begin{pmatrix} \vec{q} \\ \vec{p} \\ \vec{q}_c \\ \vec{p}_c \end{pmatrix} \rightarrow \begin{pmatrix} \vec{q} \\ \vec{p} - \delta t \nabla_{\vec{q}} H(\vec{q}, \vec{p}_c) \\ \vec{q}_c + \delta t \nabla_{\vec{p}_c} H(\vec{q}, \vec{p}_c) \\ \vec{p}_c \end{pmatrix}, \quad \phi_{H_B}^{\delta t} := \begin{pmatrix} \vec{q} \\ \vec{p} \\ \vec{q}_c \\ \vec{p}_c \end{pmatrix} \rightarrow \begin{pmatrix} \vec{q} + \delta t \nabla_{\vec{p}} H(\vec{q}_c, \vec{p}) \\ \vec{p} \\ \vec{q}_c \\ \vec{p}_c - \delta t \nabla_{\vec{q}_c} H(\vec{q}_c, \vec{p}) \end{pmatrix}, \quad (4)$$

and

$$\phi_{\omega H_C}^{\delta t} := \begin{pmatrix} \vec{q} \\ \vec{p} \\ \vec{q}_c \\ \vec{p}_c \end{pmatrix} \rightarrow \frac{1}{2} \begin{pmatrix} \begin{pmatrix} \vec{q} + \vec{q}_c \\ \vec{p} + \vec{p}_c \end{pmatrix} + R(\delta t) \begin{pmatrix} \vec{q} - \vec{q}_c \\ \vec{p} - \vec{p}_c \end{pmatrix} \\ \begin{pmatrix} \vec{q} + \vec{q}_c \\ \vec{p} + \vec{p}_c \end{pmatrix} - R(\delta t) \begin{pmatrix} \vec{q} - \vec{q}_c \\ \vec{p} - \vec{p}_c \end{pmatrix} \end{pmatrix}, \quad \text{where } R(\delta) := \begin{pmatrix} \cos(2\omega\delta t)\mathbb{I}_d & \sin(2\omega\delta t)\mathbb{I}_d \\ -\sin(2\omega\delta t)\mathbb{I}_d & \cos(2\omega\delta t)\mathbb{I}_d \end{pmatrix}. \quad (5)$$

with \mathbb{I}_d as the d -dimensional identity matrix. As shown above, the method presents 3rd-order error in δt , thus being a 2nd order method. However, higher order mappings are trivially obtainable by concatenating maps of lower order in a 'triple jump' chain:

$$\phi_l^\delta := \phi_{l-2}^{\gamma_l \delta} \circ \phi_{l-2}^{(1-2\gamma_l)\delta} \circ \phi_{l-2}^{\gamma_l \delta}, \quad (6)$$

where $\gamma_l = (2 - 2^{\frac{1}{l+1}})^{-1}$ is a scaling factor. Note that the step size $(1 - 2\gamma)$ is negative, thus integrating movement backwards, even though the order of the step is very close to 1. For the orders used here, we have $\gamma_6 = 1.12$ and $\gamma_4 = 1.17$, which do not significantly

alter the step size magnitude. We point out that that higher orders must always be even ($l = 2n$, for $n \in \mathbb{Z}$), scaling down towards the lowest one.

As addressed by Tao, the binding factor ω must consider certain limits. That is, it must not be small enough in order to introduce numerical errors given the lack of bounding between the two copies that grow in time as $O(1)$ and nor too large. It is stated that $\delta t \ll \omega^{-\frac{1}{l}}$ ensures a good approximation for a feasible ω .

Extended Hamiltonians were previously proposed for explicit methods for generic systems, particularly by Pihajoki [7], from which Tao developed its own, adding the binding term ωH_C to correct the long term conservation of symplectic area. This correction bounds the error to order $O((\delta t)^l \omega^l)$, allowing much longer integration times.

2.2 Performance evaluation

To evaluate integration precision, two functions were calculated throughout time. For the lattice model, the Hamiltonian itself was used, which is an immediate constant of the motion and corresponds to the system's energy (section 3 for details), and for the three-body model, the Jacobi constant ($J = J(x, y, p_x, p_y)$ – see section 4 for details). The other function is the symplectic non-degenerate 2-form δS between two vectors $\vec{z} = (z_1^q, \dots, z_d^q, z_1^p, \dots, z_d^p)$ and $\vec{w} = (w_1^q, \dots, w_d^q, w_1^p, \dots, w_d^p)$ in a d -degrees of freedom phase space, given by:

$$\delta S(\vec{z}, \vec{w}) := \sum_{i=1}^d dq_i \wedge dp_i = \sum_{i=1}^d (z_i^q w_i^p - z_i^p w_i^q), \quad (7)$$

which is expected to be conserved for a Hamiltonian flux, at least for integrable orbits when solved numerically [1].

For the calculation of the 2-form δS , an orbit for a given initial condition \vec{s}_0 is integrated along with a second one, slightly displaced from it with initial condition $\vec{s}_0 \rightarrow \vec{s}_0 + \vec{\delta}$, for $|\vec{\delta}| = 10^{-10}$. The 2-form will thus measure the preservation of phase space areas projected into each plane (q_i, p_i) throughout time evolution. For chaotic solutions, an exponential divergence is expected between these orbits, but the longer it takes for them to diverge, the better. For integrable orbits, a good symplectic method is expected to keep the 2-form area limited and at the lowest possible value.

It is worth mentioning that symplecticity can be only numerically achieved for regular orbits, as guaranteed by the KAM theorem, since small perturbations do not disrupt invariant tori. On the other hand, in the case of chaotic orbits, this becomes utterly impossible due to their sensitive dependence on errors. Therefore, only the true solution of the equations of motion will preserve all the invariants of the system. Even though symplectic methods present an extra conservation of the non-degenerate 2-form invariant, it may not account for all of them [1].

3 2D Optical Lattice

The first system under testing is a classical 2D optical lattice model described by the conservative separable Hamiltonian [8]:

$$H(x, y, p_x, p_y) = p_x^2 + p_y^2 + U (\cos^2(x) + \cos^2(y) + 2\alpha \cos(x) \cos(y)), \quad (8)$$

with p_x, p_y as canonical momenta, $U > 0$ an intensity parameter and $\alpha \in [0, 1]$ a coupling parameter, such that when $\alpha = 0$ the system is integrable. Units are normalized.

Optical lattices in general have been used experimentally to confine and control cold atoms for the study of new quantum states of matter [9, 10]. Theoretically, beyond the description of experiments, these Hamiltonian models are studied as both classical and quantum dynamical systems. In the classical realm particularly, they can be referred to as ‘soft billiards’, relating to the hard walls billiard models, and are mainly used to simulate anomalous diffusion of particles through periodic potentials, thus requiring long integration times.

The lattice model considered here presents a mixed phase space for a wide range of its main control parameters, namely the energy $E = H(x, y, p_x, p_y)$ and the coupling α . This allows one to fix a pair (E, α) and select different initial conditions to study both chaotic and regular behaviors from the system’s solutions. Selecting parameters $\alpha = 0.1$ and $E = 25.0$, four orbits were chosen arbitrarily, two integrable and two chaotic, with the following initial points:

- Trajectory 0 (Chaotic): $(x_0, y_0, p_{x0}, p_{y0}) = (0.00000, 1.57070, -0.100000, 2.233745)$
- Trajectory 1 (Regular): $(x_0, y_0, p_{x0}, p_{y0}) = (1.57070, 1.57070, -0.100000, 4.999000)$
- Trajectory 2 (Regular): $(x_0, y_0, p_{x0}, p_{y0}) = (1.00000, 1.57070, 2.000000, 3.893746)$
- Trajectory 3 (Chaotic): $(x_0, y_0, p_{x0}, p_{y0}) = (1.57070, 1.57070, -3.000000, 4.000000)$

The points above were integrated for a total time of $t = 300.0$, following the order of magnitude used in diffusion analysis. Since the system is spatially periodic, its position variables (x, y) are modulated within the interval $[-\pi, \pi)$ by periodic boundary conditions. Therefore, the symplectic 2-form cannot surpass a maximum amount of order 10^0 , thus it does not diverge to infinity in the literal sense, rather it oscillates with this magnitude.

As mentioned in section 2, the performance was evaluated by the deviation of the energy (δH) from its initial value and the deviation of the symplectic 2-form (δS). All the data shown for the deviations comprise the average between the four orbits at the final time simulated. However, as expected, both chaotic orbits presented divergent behavior of the symplectic area after times $t \approx 10$; thus, all data regarding 2-form conservation are taken only over regular orbits. Section 3.1 shows the algorithm performance conducted with different time steps and section 3.2 tests made with different ω values.

3.1 Time-step tests

In this section, we compare the performance of the different integration methods with Tao’s method regarding different time-steps sizes and the conservation of invariants for the lattice model. The main results obtained are compiled in table 1. For this test, all simulations using Tao’s method used $\omega = 500.0$, which yielded the best conservation results. Further tests with different ω are shown in section 3.2. Since the RKCK method has adaptive step size, its results were calculated for only one reference time step and placed in the $dt = 10^{-6}$ column.

dt	δH				δS			
	10^{-3}	10^{-4}	10^{-5}	10^{-6}	10^{-3}	10^{-4}	10^{-5}	10^{-6}
RKCK	–	–	–	2×10^{-10}	–	–	–	10^0
Störmer-Verlet	1×10^{-4}	2×10^{-6}	1×10^{-8}	1×10^{-10}	10^{-9}	10^{-9}	10^{-9}	10^{-7}
Tao ($l = 2$)	6×10^0	1×10^{-5}	1×10^{-7}	2×10^{-9}	$*10^1$	10^{-7}	10^{-7}	10^{-7}
Tao ($l = 4$)	1×10^1	1×10^{-5}	9×10^{-8}	2×10^{-8}	$*10^1$	10^{-7}	10^{-7}	10^{-7}
Tao ($l = 6$)	8×10^0	1×10^{-5}	8×10^{-8}	3×10^{-8}	$*10^1$	10^{-7}	10^{-7}	10^{-7}

Table 1: Energy (δH) and symplectic 2-form (δS) deviations for different integration algorithms in different magnitude orders of time steps dt . The * mark indicates that orbit 3 presented divergence whereas orbit 2 remained with δS conserved.

One of the main features shown in table 1 is the lack of improvement in both energy and symplectic area in Tao’s method when increasing the order l , particularly for δS , which remained constant at 10^{-7} (for $dt \leq 10^{-4}$). This same level of deviation was found in almost all simulations made, probably due to the fact that higher order mappings comprise only smaller steps of the order 2 map, halving the step size dt for each order decrement. Therefore, up to order 6 this divides the original step size only by 4, thus not increasing its magnitude significantly. Nevertheless, as mentioned, this same level of conservation was found even for different binding factors, time step or order alike, possibly being related to a more fundamental reason.

In addition to the results shown in table 1, an extension of the integration time was made to $t = 3000$, for the cases $dt = 10^{-4}$ and $dt = 10^{-5}$. The purpose was to evaluate whether integration order delays the time required for energy deviation. However, no such behavior was found and energy deviations were bounded within the same magnitude for $dt = 10^{-5}$ whereas for $dt = 10^{-4}$ it diverged for times close to $t = 1000$. Divergent runs did not present any pattern or delay of divergence time with the increment of integration order.

In general, besides the smallest time step used ($dt = 10^{-3}$), Tao’s method presented similar conservation performance as Störmer-Verlet. As expected, both symplectic methods present significantly lower performance in energy conservation magnitude when compared to RKCK, even though the latter presents secular growth and does not conserve symplectic area at all. The best performance found for symplectic methods had bounded energy fluctuations in the simulated time interval (exceptions will be mentioned in section 3.2).

The discrepancy between Verlet and Tao for $dt = 10^{-3}$ could be fixed with a different choice of ω , since this parameter is directly related to the time-step selected. Even though the selected value of $\omega = 500$ is well below the upper threshold $\delta t \ll \omega^{-\frac{1}{l}} = 0.35$ (for $l = 6$), it may possibly be lower than a bottommost threshold.

In addition to conservation itself, the CPU time required for the simulations is also shown in table 2. We point out that the computation time measured includes writing to file, symplectic 2-form and energy evaluations, although this process is common for all tests ran and for all methods, and may not interfere in the direct comparison between them. Furthermore, among the methods compared, Verlet and Tao were implemented manually with little to no optimization, whereas RKCK was used from the highly optimized GSL library [11], and being an adaptive step size method it has direct advantages from the other two.

dt	CPU time			
	10^{-3}	10^{-4}	10^{-5}	10^{-6}
RKCK [†]	-	-	-	4sec
Störmer-Verlet	2sec	28sec	4min 57sec	47min 24sec
Tao ($l = 2$)	3sec	29sec	5min 10sec	50min 11sec
Tao ($l = 4$)	4sec	36sec	6min 1sec	59min 34sec
Tao ($l = 6$)	6sec	52sec	8min 43sec	87min 47sec

Table 2: CPU time required for integration of the orbits for different methods and different time steps. Parameters are the same used for the data in table 1.

The tests conducted here should not be considered a rigorous benchmark, but rather as extra information providing the order of magnitude at which numerical algorithms may work. In particular, one may note that second-order Tao’s method has a performance close to Verlet with similar CPU times, thus making it a good alternative. The slightly higher time in Tao’s algorithm can be credited to the evaluation of sines and cosines, requiring considerable extra computation time when performed excessively along with the integration of the additional copied variables. Nevertheless, the method can be regarded as equivalent to the simple algorithm of Verlet, along with the extra feature of being generically applicable to non-separable systems.

3.2 Binding factor tests

Analogously to the time step size tests previously shown, the performance of Tao’s method for a series of binding parameter ω is shown in tables 3, 4 and 5 for time steps of $dt = 10^{-4}$, $dt = 10^{-5}$ and $dt = 10^{-6}$, respectively. As pointed out in section 2, the choice of dt is dependent on the value of ω and vice-versa, thus its testing requires a series of different magnitude values for both of them.

Besides the smaller time step used ($dt = 10^{-4}$), which presented good conservation only for the middle range binding value ($\omega = 500$), in all cases energy was conserved to at least order 10^{-7} . However, for the smaller step size ($dt = 10^{-6}$), several cases showed a clear linear growth of deviation for all orbits selected, the so-called secular deviation, even though its deviation did not surpass 10^{-7} over 300 time units. Figure 1 shows the comparison between a regular case with bounded energy and one with secular growth.

$dt = 10^{-4}$	δH			δS		
ω	50	500	5000	50	500	5000
$l = 2$	2×10^1	1×10^{-5}	1×10^1	1×10^{-7}	1×10^{-7}	1×10^{-7}
$l = 4$	1×10^1	1×10^{-5}	9×10^0	1×10^{-7}	1×10^{-7}	1×10^{-7}
$l = 6$	1×10^1	1×10^{-5}	9×10^0	1×10^{-7}	1×10^{-7}	1×10^{-7}

Table 3: Energy (δH) and symplectic 2-form (δS) deviations for different binding values ω for Tao’s method with time step $dt = 10^{-4}$.

Regarding the conservation of the symplectic 2-form, for all cases, regular orbits presented the same deviation level, no greater than 10^{-7} regardless of integration order or binding value. Even in cases where energy deviation presented secular growth, δS remained at the same conservation level. In most cases, an increase in ω does not improve

energy conservation up to $t = 300$ but it helped stop linear growth deviation. This indicates that some values may be too close to the bottom limit ω_0 , thus it is recommendable to take higher values, since these are safely below the upper limit of $dt \ll \omega^{-\frac{1}{l}} \approx 0.3$.

$dt = 10^{-5}$	δH			δS		
ω	50	500	5000	50	500	5000
$l = 2$	1×10^{-7}	1×10^{-7}	1×10^{-7}	1×10^{-7}	1×10^{-7}	1×10^{-7}
$l = 4$	1×10^{-7}	1×10^{-7}	1×10^{-7}	1×10^{-7}	1×10^{-7}	1×10^{-7}
$l = 6$	9×10^{-8}	1×10^{-7}	1×10^{-7}	1×10^{-7}	1×10^{-7}	1×10^{-7}

Table 4: Energy (δH) and symplectic 2-form (δS) deviations for different binding values ω for Tao's method with time step $dt = 10^{-5}$.

Unexpectedly, for $l = 6$, the conservation became slightly worse as we increased ω , although in all cases the limit $dt \ll \omega^{-\frac{1}{l}}$ was satisfied. For all ω , the upper limit is given by $50^{-1/6} = 0.52$, $500^{-1/6} = 0.3549$ and $5000^{-1/6} = 0.2418$, thus making these results counter intuitive since as we increase ω we move away from the unspecified bottom limit ω_0 , being safely inside the 'limits' for dt .

$dt = 10^{-6}$	δH			δS		
ω	50	500	5000	50	500	5000
$l = 2$	$*5 \times 10^{-9}$	$*3 \times 10^{-9}$	2×10^{-9}	$*1 \times 10^{-7}$	$*1 \times 10^{-7}$	1×10^{-7}
$l = 4$	$*5 \times 10^{-9}$	$*3 \times 10^{-9}$	$*2 \times 10^{-9}$	$*1 \times 10^{-7}$	$*1 \times 10^{-7}$	$*1 \times 10^{-7}$
$l = 6$	$*4 \times 10^{-9}$	3×10^{-8}	1×10^{-8}	1×10^{-7}	1×10^{-7}	1×10^{-7}

Table 5: Energy (δH) and symplectic 2-form (δS) deviations for different binding values ω for Tao's method with time step $dt = 10^{-6}$. Fields marked by * presented secular growth of energy for all cases.

In the previous section, all data exposed was made for $\omega = 500$, since this parameter yielded the best result considering all time steps. Notwithstanding, the best results for energy conservation were obtained for $\omega = 5000$ and $dt = 10^{-6}$, however not for arbitrary orders. In general, changes in the binding factor did not alter much the order of conservation for $dt = 10^{-5}$ and $dt = 10^{-6}$, but implied secular growth in the latter. Higher sensitivity was found for $dt = 10^{-4}$.

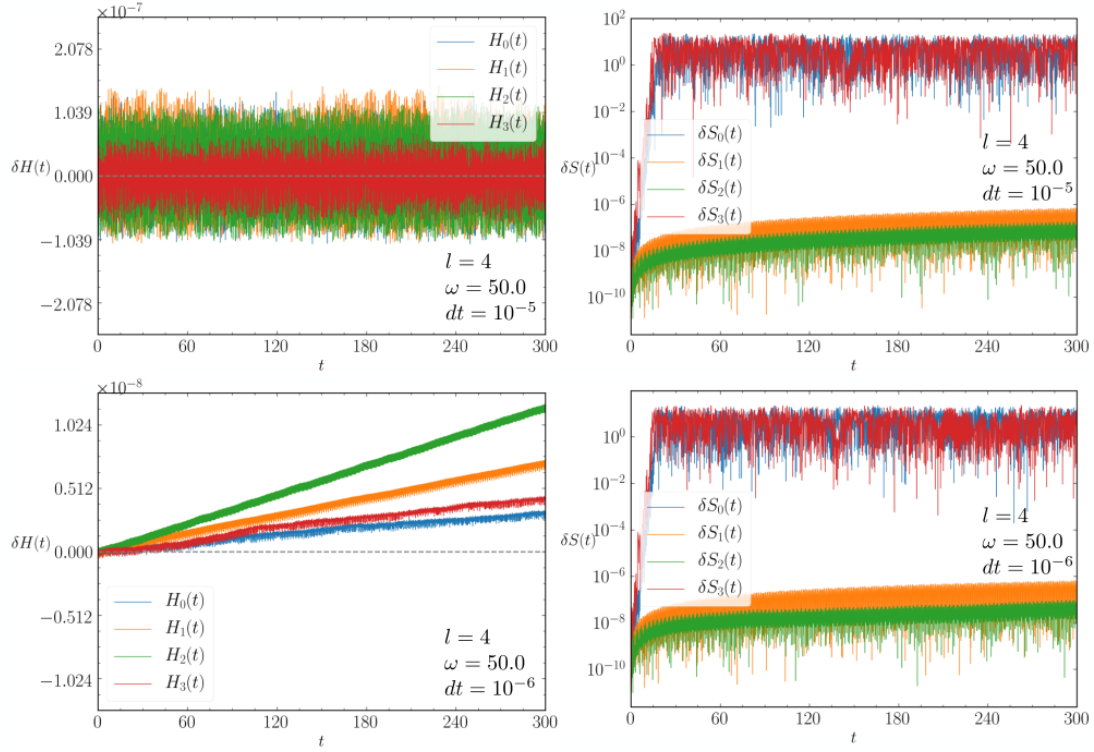


Figure 1: (Top row) Energy deviation δH (left) and symplectic 2-form δS (right) along time for 4th order Tao's method with $\omega = 50.0$ and $dt = 10^{-5}$ depicting limited growth and oscillatory fluctuations. (Bottom row) The same as the above but for smaller time-step $dt = 10^{-6}$ depicting secular growth of energy, at least up to the time interval considered.

4 Restricted three-body problem

One of the simplest examples of n -body planetary systems, yet still presenting complex solutions, is given by the restricted three-body problem. This classical formulation considers two heavy masses and a probe particle with negligible mass compared to the more massive ones, moving along the gravitational potential of the two massive bodies (figure 2). This scenario can possibly represent a triad of a star, a planet and a small moon, or a planet, its moon and a satellite.

The most common representation of the system is from a rotational frame of reference, with the heavy bodies fixed along the $y = 0$ axis, 1 space unity apart from each other. This relates to two main aspects of the model. First, that the heavy bodies orbit around its center of mass with the same angular velocity n (which is also the velocity of the rotating frame), and second, that a unitary length scale is settled. In this setup, the masses are scaled so that the reduced mass is unitary, *i.e.*, $\mu = G(\mu_1 + \mu_2) = 1$, where G is the gravitational constant and $\mu_i = m_i / (m_1 + m_2)$ is the reduced mass of the massive bodies [12, 13].

The probe dynamics is thus restricted to be coplanar with the massive bodies and its movement dictated by a potential $\Omega(x, y)$, resulting from the superposition of the individual gravitational interactions with the two heavy bodies and an term accounting for the centrifugal force due to the rotating frame:

$$\Omega(x, y) = \frac{n}{2} (x^2 + y^2) + \frac{\mu_1}{\sqrt{(x + \mu_2)^2 + y^2}} + \frac{\mu_2}{\sqrt{(x - \mu_1)^2 + y^2}} \quad (9)$$

In the Hamiltonian formulation, one can write the particle's canonical variables as its position and a pair of conjugated momenta (p_x, p_y) , and the system Hamiltonian written as

$$H(x, y, p_x, p_y) = -2J(x, y, p_x, p_y) \quad (10)$$

where

$$J(x, y, p_x, p_y) = 2\Omega(x, y) - (p_x + y)^2 - (p_y - x)^2 \quad (11)$$

It is worth mentioning that since the coordinate system (x, y) is rotating, the Hamiltonian function 10 does not correspond to the particle's energy. Instead, it corresponds to the so called Jacobi function J , which is itself a constant of motion.

Analogously to the procedure shown in section 3 for the lattice model, we selected the system parameters with a Jacobi constant of $J = 3.1843$ and reduced masses $\mu_1 = 0.9879$ and $\mu_2 = 1 - \mu_1 = 0.0121$. In accordance with these parameters, four initial conditions were selected:

- Trajectory 0 (Chaotic): $(x_0, y_0, p_{x0}, p_{y0}) = (1.080000, 0.000000, -0.080000, 1.300003)$
- Trajectory 1 (Regular): $(x_0, y_0, p_{x0}, p_{y0}) = (0.600000, 0.000000, 0.000000, 1.282517)$
- Trajectory 2 (Regular): $(x_0, y_0, p_{x0}, p_{y0}) = (0.300000, 0.000000, 0.000000, 2.108413)$
- Trajectory 3 (Chaotic): $(x_0, y_0, p_{x0}, p_{y0}) = (0.550000, 0.000000, 0.000000, 1.246951)$

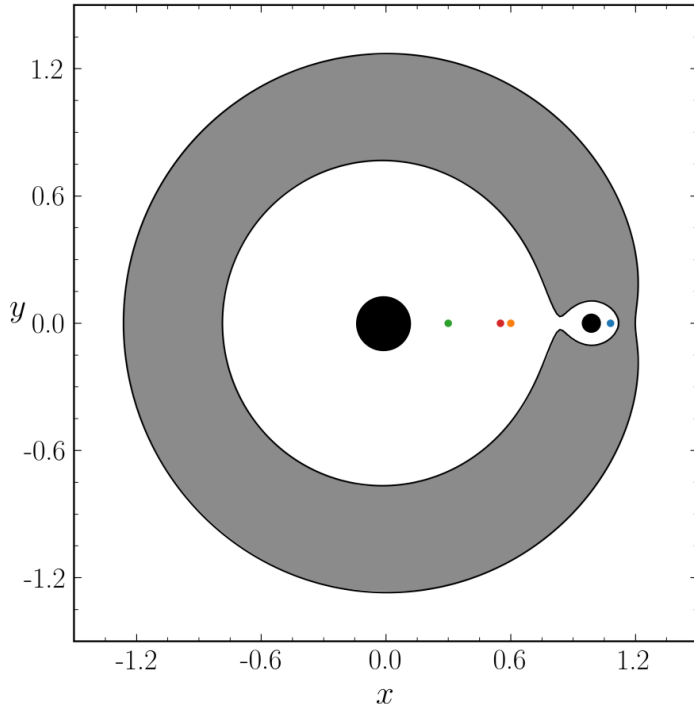


Figure 2: Spatial plot of the planar restricted three-body model scheme. Black circles indicate the massive bodies and the colored dots the initial conditions used. The gray area corresponds to Hill's region, where the probe particle is not allowed to enter due to the restriction $2\Omega(x, y) > J$, bounded by the zero-velocity curve. For the parameters selected, $(J = 3.1843, \mu_1 = 0.9879, \mu_2 = 0.0121)$, all orbits are enclosed and cannot escape the surroundings of the massive bodies, being allowed to move only within the inner white area. It can orbit either the heavier or the lighter mass or transit between the two.

A total time of $t = 1000.0$ was used for the integration. The initial conditions were selected such that two of them are chaotic and two regular. None of them collide with either of the massive bodies, in the sense that their distance to any of the divergence points does not get smaller than 10^{-6} . Thus, integration can be performed without the necessity of renormalization techniques.

4.1 Performance tests

Similar to what was done for the lattice model in section 3, this section presents the performance comparison between different integration methods and Tao's symplectic one for a series of its parameters. Different magnitudes of time step, binding factor ω , and integration order were considered for Tao's method. As before, integration performance was evaluated by the deviations of symplectic 2-form (δS) and Jacobi constant (δJ), which is a constant of motion for the restricted three-body problem [13]. As will be discussed shortly, Tao's second-order ($l = 2$) yielded the best performances, thus, for simplicity, results for higher orders were suppressed.

The results were divided by the Jacobi constant, as shown in table 6, and symplectic 2-form, shown in table 7. All data displayed for Jacobi constant comprises the average of all four orbits simulated, whereas those for the symplectic 2-form consider only the two regular orbits. Cases in which divergence occurred are marked by an asterisk (figure 3). For the two other methods used for comparison, Störmer-Verlet and RKCK, since they have no relation with a binding factor, their results are placed in a single column in order to be displayed along with Tao's results.

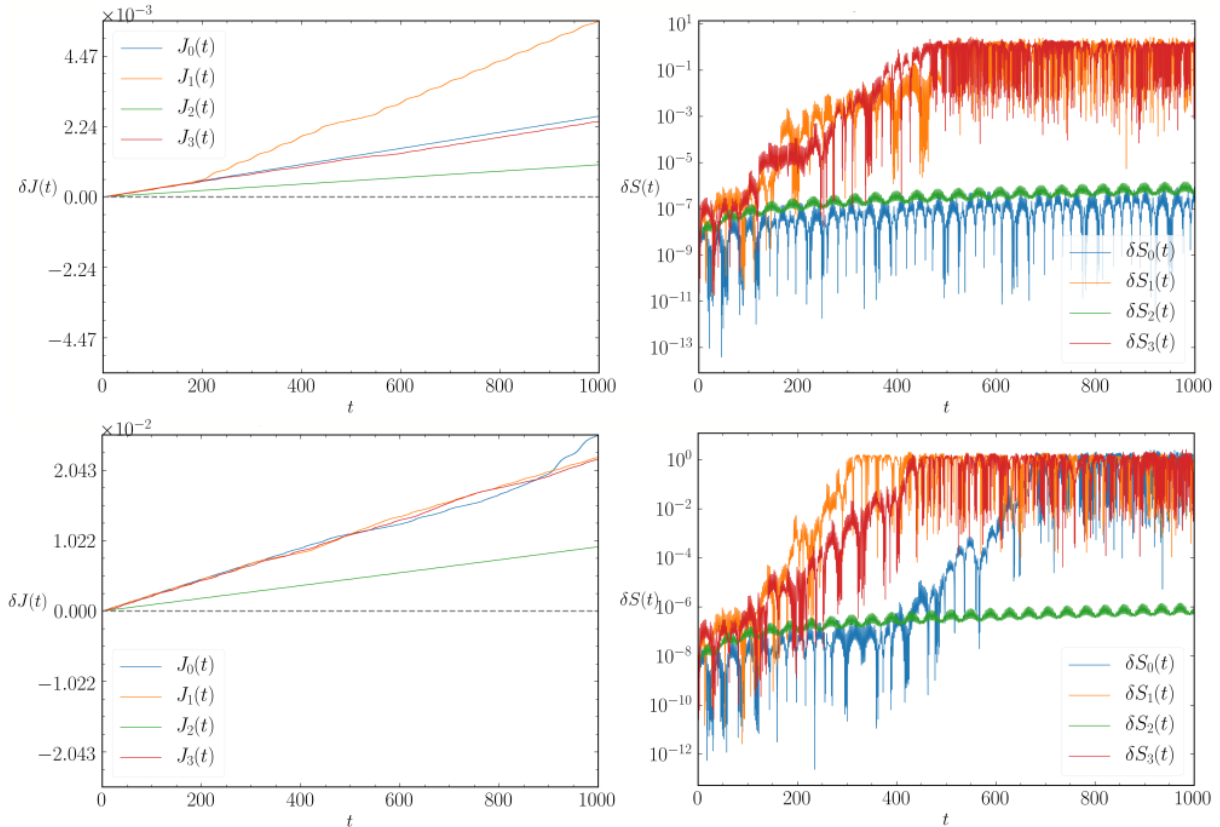


Figure 3: (Top row) Jacobi constant δJ (left panel) and symplectic 2-form δS (right panel) deviations for the four orbits simulated for the best performance found (parameters: $l = 2$, $\omega = 5 \times 10^6$, $dt = 10^{-6}$). (Bottom row) The same as the top row but for a case presenting deviation (parameters: $l = 6$, $\omega = 5 \times 10^4$, $dt = 10^{-6}$).

As a general trend, both symplectic methods presented poor conservation of the Jacobi constant, not being better than 10^{-3} (see table 6). Even though Störmer-Verlet is not applicable to non-separable systems, it was used here to compare with the poor performance found by Tao’s method. For comparison, RKCK yielded a deviation of 10^{-14} . Moreover, in the lattice model previously discussed, the same comparison between symplectic and RKCK methods showed the difference in magnitude of two orders. No detailed investigation was made on this difference between the two systems, however, it seems related to the non-separability of the three-body system motion equations. Although the method is supposed to handle this kind of scenario, it presented a similar behavior then Störmer-Verlet which is not expected to.

Regarding the variation of the binding factor ω , the magnitudes selected for testing here showed the best results. Nevertheless, a more extensive investigation for values within a narrow range of the orders of magnitude considered here may possibly yield better results. Even though no significant variation was found for the binding factor for a given time-step, this shows that depending on the integration order, it can disrupt conservation. For the selected binding factors, the lower estimated upper limit for the time-step ($\delta t \ll \omega^{-\frac{1}{l}}$) is for $l = 2$ and $\omega = 5 \times 10^6$, and it is given by 4.4×10^{-4} , thus still one order of magnitude higher than the time-step used.

Given the low performance, larger time-steps were not considered since no increment is expected for these cases, particularly since a higher magnitude approaches the upper limit of the time-step. For lower magnitudes, although it shall improve conservation, it

were not tested due to its long computational cost for the symplectic algorithms used here. For the magnitudes selected, $dt = 10^{-5}$ and $dt = 10^{-6}$, an expected improvement of one order of magnitude is achieved with the smaller one. However, as seen for the lattice model, no significant enhancement is seen for higher integration orders.

dt	δJ					
	10^{-5}			10^{-6}		
ω	5×10^4	5×10^5	5×10^6	5×10^4	5×10^5	5×10^6
RKCK	–	–	–	–	–	10^{-14}
Störmer-Verlet	–	–	4×10^{-2}	–	–	3×10^{-3}
Tao ($l = 2$)	2×10^{-2}	2×10^{-2}	2×10^{-2}	2.6×10^{-3}	2.8×10^{-3}	2.6×10^{-3}

Table 6: Jacobi constant deviations (δJ) for different integration algorithms for different magnitudes of time step dt and binding factor ω (regarding Tao’s method only).

All tested cases showed secular deviation of the energy (as illustrated in figure 3), with no bounded oscillations as seen for the 2D lattice model, even though some of them still showed logarithmic deviation of the symplectic area. However, divergence of symplectic 2-form was still commonly found. Particularly for $dt = 10^{-5}$, all cases showed divergence of the symplectic area for at least one of the regular orbits.

Similar to the results on the lattice model, conservation of symplectic area did not present any improvement in magnitude, remaining at a constant level of 10^{-7} regardless of variation of ω , dt or l . The main difference seems to affect the conservation itself, which shows complete divergence.

dt	δS					
	10^{-5}			10^{-6}		
ω	5×10^4	5×10^5	5×10^6	5×10^4	5×10^5	5×10^6
RKCK	–	–	–	–	–	10^{-1}
Störmer-Verlet	–	–	10^{-6}	–	–	10^{-7}
Tao ($l = 2$)	$10^{-7}(*)$	$10^{-7}(*)$	$10^{-7}(*)$	10^{-7}	10^{-7}	10^{-7}

Table 7: Symplectic 2-form deviations (δS) for different integration algorithms for different magnitudes of time steps dt and binding factor ω (regarding Tao’s method only). Cases marked with (*) presented secular divergence on one of the regular orbits.

5 Final Remarks

The series of tests performed here presented diverse results for the two systems selected: the 2D lattice classical model and the restricted three-body problem. For the 2D lattice model, good performance was achieved for some parameters of Tao’s algorithm (time-step, binding factor, and integration order), with bounded energy deviations of the order of 10^{-9} and the symplectic 2-form preserved at the order of 10^{-7} . The results for the lowest order ($l = 2$) were comparable in both performance and CPU time to the Störmer-Verlet. When compared to RKCK, an expectedly lower energy conservation was achieved but still at an acceptable level.

For the three-body problem, poor performance in the conservation of the Jacobi constant was found for all binding factors, time-step and integration order values considered. Even though symplectic 2-form was kept conserved to order 10^{-7} , many cases still diverged along with Jacobi’s constant, which did not present deviations smaller than order 10^{-3} . For the tests on this system regarding the binding factor ω , no bounded energy preservation was found, raising the question of whether a narrow interval of ω values, within the magnitude values selected here, could yield a better result than the ones obtained.

In general for both systems, higher orders of Tao’s method, up to the sixth, did not improve conservation of either the Hamiltonian constants (energy and Jacobi constant) or the symplectic 2-form. Moreover, this also implies that the construction of an adaptive time step version of the algorithm may not be trivially achieved by comparing step sizes of different precision for error evaluation.

Given the higher dependency of performance with the binding factor chosen, the use of Tao’s method requires special attention to the binding factor. As shown in section 3.2 for the lattice system, values that are too low can easily lead to secular energy deviation or even complete lack of conservation. For this system, with step sizes of order $dt = 10^{-5}$, a large range of values covering at least two orders of magnitude ($\omega > 50$) showed good conservation results.

Even though Tao’s method does not aim at speed, but rather aims at symplecticity and ease of implementation for generic Hamiltonian systems, its CPU time is drastically slower when compared to the RKCK method. We recommend its use for integrating single orbits that require the conservation of symplectic area. However, further benchmarks and code optimization could provide better information and the possibility of improved performance and calculation of averages over full phase spaces, for example. We call attention to the binding factor choice, since different initial conditions may require considerably different values, possibly with complete lack of conservation.

Acknowledgments

M. Lazarotto would like to acknowledge Vitor M. Oliveira for valuable discussions on symplectic integration and on the restricted three-body problem. The authors also acknowledge the financial support from the Brazilian federal agencies CNPq, grants 302665/2017-0 and 141750/2019-7 and the São Paulo Research Foundation (FAPESP, Brazil), grant 2018/03211-6.

References

- [1] T. J. Stuchi. Symplectic integrators revisited. *Brazilian Journal of Physics*, 32(4):958–979, 2002.
- [2] J. R. Cash and A. H. Karp. A variable order Runge-Kutta method for initial value problems with rapidly varying right-hand sides. *ACM Transactions on Mathematical Software*, (16):201–222, 1990.
- [3] E. Fehlberg. Low-order classical Runge-Kutta formulas with stepsize control and their application to some heat transfer problems. *Nasa technical report*, R-315, 1969.
- [4] J. R. Dormand and P. J. Prince. A family of embedded Runge-Kutta formulae. *Journal of Computational and Applied Mathematics*, 6(1):19–26, 1980.
- [5] E. Hairer; C. Lubich and W. Gerhard. Geometric numerical integration illustrated by the stoermer-verlet method. *Acta Numerica*, 12:399–450, 2003.
- [6] M. Tao. Explicit symplectic approximation of nonseparable hamiltonians algorithm and long time performance. *Arkiv*, 2016.
- [7] Pauli Pihajoki. Explicit methods in extended phase-space for inseparable Hamiltonian problems. *Celest Mech Dyn Astr*, 121:211–231, 2015.
- [8] Eric Horsley; Stewart Koppell and L. E. Reichl. Chaotic dynamics in a two-dimensional optical lattice. *Physical Review E*, 89(012917):1–5, 2014.
- [9] I. Bloch. Ultracold quantum gases in optical lattices. *Nature Physics*, 1:23–30, 2005.
- [10] I. Bloch; J. Dalibard and W. Zwerger. Many-body physics with ultracold gases. *Reviews of modern physics*, 80:885–964, 2008.
- [11] Galassi et al. GNU Scientific Library Reference Manual (2nd ed.) ISBN 0954161734.
- [12] Carl D. Murray and Stanley F. Dermott. *Solar System Dynamics*. Cambridge University Press, 2009.
- [13] V. M. de Oliveira; P. A. Souza-Silva and I. L. Caldas. Order-chaos-order and invariant manifolds in the bounded planar Earth–Moon system. *Celest Mech Dyn Astr*, 132(51), 2020.

Appendix

A code implementation made in C/C++ programming language is shown below, along with a minimal example on how to use it. The simplicity of the method’s algorithm makes it easy to port to other languages, requiring basic computational features. The dynamical equations used for the 2D optical lattice and the three-body model are also available at the final subsection, allowing for complete reproduction of the tests conducted here. The full code can be retrieved at: <https://github.com/matheuslazarotto/SymplecticTao>.

Minimal usable example

A minimal setup example to integrate an orbit from a initial condition x_0 , y_0 , px_0 , py_0 for a total time `run_time` is presented here. It starts by showing the system's dynamical functions defined in `system_functions()`, allowing the use of external arguments, *i.e.*, constants or parameters of any sort stored in an array `*args`. Then, `main()` function is where integration is ran up to `run_time`, in time steps of size `dt`, while evolving the array with the dynamical variables (and in parallel the copy variables `variables_copy`), along with other parameters required by the method, namely the `order`, `omega` and `gamma`.

This example considers a generic conservative and separable Hamiltonian function with two degrees of freedom (therefore a 4D dynamical system), with cartesian coordinates (x,y,px,py) and motion equations given by the functions: `dqxdt()`, `dqydt()`, `dpxdt()`, `dpydt()`. Although, this implementation is trivially generalizable to any number of degrees of freedom. This pictoric example assumes two constant parameters (k and m), stored in the array `args[] = {k, m}`.

The explicit code for Tao's method function `step_ode_step_symplectic()` is displayed further in this appendix.

```
int system_functions(double t, const double var[], double functions[], void *args)
{
    (void)(t); // Avoid unused parameter warning
    double *par = (double *)args;
    double k = par[0];
    double m = par[1];

    f[0] = dqxdt(var[2], m);
    f[1] = dqydt(var[3], m);
    f[2] = dpxdt(var[0], var[1], k);
    f[3] = dpydt(var[1], var[0], k);

    return 0;
}

int main()
{
    const int system_dimension = 4;
    const double run_time = 100.0;
    const double x0 = 1.0;
    const double y0 = 1.0;
    const double px0 = 5.0;
    const double py0 = 1.0;
    const double k = 1.0;
    const double m = 1.0;
    const double args[] = {k, m};
    const double dt = 1e-4;
    double time = 0.0;
    double variables = {x0, y0, px0, py0};
    double variables_copy[] = {x0, y0, px0, py0};
```

```

const int order = 4;
const double omega = 100.0;
const double gamma = 1.0 / (2.0 - pow(2.0, 1 / (order + 1)));
const bool lowest = (order == 2) ? true : false;

/* Integration loop */
while (t <= run_time)
{
    ode_step_symplectic(variable, variable_copy, t, dt,
                        omega, gamma, system_dimension,
                        order, lowest, args, system_functions);
}
}

```

Method implementation

Below is the implementation of the functions required to run the integration algorithm. The main function used is `ode_step_symplectic()`, which evolves the system variables (and its copy in parallel) for one time step dt , for a given integration order, binding rotation ω , and time γ parameters.

The `ode_step_symplectic()` function calls itself recursively when applying ‘triple jumps’, (see section 2), diminishing to lower orders (in even steps) until the lowest one (2) is reached, where the last ‘triple jump’ chain is called as `ode_step_symplectic_lowest()`. However, if one applies the method with order 2, it is required to be different of when the lowest case (order = 2) is reached from the downscaling when recursively called from a higher order method. When one simply wants to integrate using order 2, no triple jump is required, only the regular mapping (eq. 3), whereas when reaching order 2 by downscaling, a triple jump of order 2 ϕ mappings must be called (eq. 6). For this purpose, a boolean flag `lowest` is set to `true` in case only direct order 2 integration is made, or `false` when higher order downscaling must be used. The partial mappings ϕ_A , ϕ_B and ϕ_C are separately implemented.

```

void ode_step_symplectic(double var[], double var_copy[], double &t, double dt,
                        double w, double gamma, unsigned int system_dim, int order,
                        bool lowest, double *args, int (*system_function)(double t,
                        const double s[], double f[], void *args))
{
    /* Recursively call ‘triple jumps’ of Phi maps down to the lowest order (2) */
    if (lowest)
    {
        ode_step_symplectic_lowest(var, var_copy, t, dt, w, system_dim,
                                    args, system_function);
    }
    else
    {
        order -= 2;
        double dt_s = gamma * dt;
        double dt_m = (1.0 - 2.0 * gamma) * dt;
        if (order > 2)

```

```

    {
        double local_gamma = 1.0 / (2.0 - pow(2.0, 1 / (order + 1)));
        ode_step_symplectic(var, var_copy, t, dt_s, w, local_gamma, system_dim,
                            order, lowest, args, system_function);
        ode_step_symplectic(var, var_copy, t, dt_m, w, local_gamma, system_dim,
                            order, lowest, args, system_function);
        ode_step_symplectic(var, var_copy, t, dt_s, w, local_gamma, system_dim,
                            order, lowest, args, system_function);
    }
    else if (order == 2)
    {
        ode_step_symplectic_lowest(var, var_copy, t, dt_s, w, system_dim,
                                   args, system_function);
        ode_step_symplectic_lowest(var, var_copy, t, dt_m, w, system_dim,
                                   args, system_function);
        ode_step_symplectic_lowest(var, var_copy, t, dt_s, w, system_dim,
                                   args, system_function);
    }
}
}

```

```

void ode_step_symplectic_lowest(double var[], double var_copy[], double &t,
                                double dt, double w, unsigned int system_dim,
                                double *args, int (*system_function)(double t,
                                const double s[], double f[], void *args))
{
    double step = 0.5 * dt;
    double f[system_dim];
    double f_copy[system_dim];

    /** Evaluate derivatives for Pa **/
    system_function(0.0, var, f, args);
    system_function(0.0, var_copy, f_copy, args);
    /** Apply Pa **/
    phi_a(var, var_copy, f, f_copy, step, system_dim);

    /** Evaluate derivatives for Pb **/
    system_function(0.0, var, f, args);
    system_function(0.0, var_copy, f_copy, args);
    /** Apply Pb **/
    phi_b(var, var_copy, f, f_copy, step, system_dim);

    /** Apply Pc **/
    phi_c(var, var_copy, dt, w, system_dim);

    /** Evaluate derivatives for Pb **/
    system_function(0.0, var, f, args);
    system_function(0.0, var_copy, f_copy, args);
}

```

```

    /** Apply Pb **/
    phi_b(var, var_copy, f, f_copy, step, system_dim);

    /** Evaluate derivates for Pa **/
    system_function(0.0, var, f, args);
    system_function(0.0, var_copy, f_copy, args);
    phi_a(var, var_copy, f, f_copy, step, system_dim);

    t += dt;
}

void phi_a(double var[], double var_copy[], const double function[],
           const double function_copy[], double step, unsigned int system_dim)
{
    unsigned int n = system_dim / 2;

    for (unsigned int k = 0; k < n; k++)
    {
        var[k+n] += step * function[k+n];
        var_copy[k] += step * function_copy[k];
    }
}

void phi_b(double var[], double var_copy[], const double function[],
           const double function_copy[], double step, unsigned int system_dim)
{
    unsigned int n = system_dim / 2;
    for (unsigned int k = 0; k < n; k++)
    {
        var[k] += step * function[k];
        var_copy[k+n] += step * function_copy[k+n];
    }
}

void phi_c(double var[], double var_copy[], double step, double w,
           unsigned int system_dim)
{
    int n = system_dim / 2;
    double cwd = cos(2.0 * w * step);
    double swd = sin(2.0 * w * step);
    double tmp_var[system_dim];
    double tmp_var_copy[system_dim];

    for (int k = 0; k < n; k++)
    {
        tmp_var[k] = 0.5 * (var[k] + var_copy[k] +
                           cwd * (var[k] - var_copy[k]) +
                           swd * (var[k+n] - var_copy[k+n]));
    }
}

```

```

tmp_var[k+n] = 0.5 * (var[k+n] + var_copy[k+n] -
                    swd * (var[k] - var_copy[k]) +
                    cwd * (var[k+n] - var_copy[k+n]));
tmp_var_copy[k] = 0.5 * (var[k] + var_copy[k] -
                       cwd * (var[k] - var_copy[k]) -
                       swd * (var[k+n] - var_copy[k+n]));
tmp_var_copy[k+n] = 0.5 * (var[k+n] + var_copy[k+n] +
                          swd * (var[k] - var_copy[k]) -
                          cwd * (var[k+n] - var_copy[k+n]));
}

for (int k = 0; k < system_dim; k++)
{
    var[k] = tmp_var[k];
    var_copy[k] = tmp_var_copy[k];
}
}

```

Equations of motion

Despite being simple to obtain, the equations of motion used for the tests are made available in order to allow the faithful reproduction of the results shown here.

```

int system_function_2d_optical_lattice(double t, const double s[],
                                       double f[], void *args)
{
    (void)(t); // Avoid unused parameter warning
    double *par = (double *)args;
    double a = par[0];
    double U = par[1];

    f[0] = 2.0 * s[2];
    f[1] = 2.0 * s[3];
    f[2] = 2.0 * U * sin(s[0]) * (cos(s[0]) + a * cos(s[1]));
    f[3] = 2.0 * U * sin(s[1]) * (cos(s[1]) + a * cos(s[0]));

    return 0;
}

int system_function_three_body(double t, const double s[],
                              double f[], void *args)
{
    (void)(t); // Avoid unused parameter warning
    double *par = (double *)args;
    double n = par[0];
    double mu_1 = par[1];
    double mu_2 = par[2];

    f[0] = s[2] + s[1];
}

```

```

f[1] = s[3] - s[0];
double r1_3rd = pow(sqrt((s[0] + mu_2) * (s[0] + mu_2) + s[1] * s[1]), 3);
double r2_3rd = pow(sqrt((s[0] - mu_1) * (s[0] - mu_1) + s[1] * s[1]), 3);
f[2] = s[3] - s[0] + n * n * s[0] - mu_1 * (s[0] + mu_2) / r1_3rd -
      mu_2 * (s[0] - mu_1) / r2_3rd;
f[3] = -s[2] - s[1] + n * n * s[1] - (mu_1 / r1_3rd + mu_2 / r2_3rd) * s[1];

return 0;
}

```

Full code available in: <https://github.com/matheuslazarotto/SymplecticTao>.